Synergic effect among activated carbon/sulphur-assisted graphitic carbon nitride for enhanced photocatalytic activity

Asif Hussain [a b c], Muhammad Tahir [d], Wei Yang [e], Renlong Ji [f], Kewang Zheng [g], M. Umer [c], S yed Muhammad Ahmad [c], M. Boota [c], Ahmed Iftikhar [c], Ali Raza [c], Zia Ur Rehman [a b], Naushad Ahmad [h], Rosa Busquets [i], Jianhua Hou [a b *], Xiaozhi Wang [a b *]

[a]College of Environmental Science and Engineering, Yangzhou University, Yangzhou 225127, PR China

[b]College of Physical Science and Technology, Yangzhou University, Yangzhou 225127, PR China

[c]Department of Physics, The University of Lahore, Lahore, Pakistan

[d]Department of Physics, University of Education, Pakistan

[e]Beijing System Design Institute of Electro-Mechanic Engineering, Beijing 100005, PR China

[f]College of Materials Science and Engineering, Yantai Nanshan University, No.12, Daxue Road, Donghai Tourist Resort, Longkou City, Shandong Province 265713, PR China

[g]School of Chemistry and Materials Science, Hubei Engineering University, Xiaogan, China

[h]Department of Chemistry, College of Science, King Saud University, Riyadh 11451, Saudi Arabia

[i]School of Life Sciences, Pharmacy and Chemistry, Kingston University London, Penrhyn Road, Kingston-upon-Thames, Surrey KT1 2EE, UK

*Corresponding authors at: College of Environmental Science and Engineering, Yangzhou University, Yangzhou 225127, PR China.

E-mail addresses: jhhou@yzu.edu.cn (J. Hou), xzwang@yzu.edu.cn (X. Wang)

Abstract

Synthesis of 2D carbon-based layered structures materials is highly desirable for higher-photocatalytic activities. Here in this regard, we use commercially exhausted urea for the fabrication activated carbons and graphitic carbon nitride (GCN) layered structures doped with sulphur to accumulate activated carbon with S for pollutants degradation using the thermal decomposition method. The synthesized material contains activated carbon in a small amount, which does not accumulate with nitrogen to form GCN and cause a higher energy bandgap (3.31 eV - 3.38 eV). However, through S, we have modified the bandgap and reduced it to (2.84 eV - 3.06 eV) for visible light. The S with activated carbon system along with GCN enhances the synergetic contribution in degradation. The reaction constant (K) is increased from (3.5×10^{-3} - 4.1×10^{-2}) owing to synergic effect. Most notably, a significant amount of sulphur accumulated with activated carbon and GCN, altered the charge transfer route and enhanced optical absorption and higher photocatalytic activity, and i considered a novel approach for environmental remediation.

Keywords: Photo-catalysis; Sulphur assisted GCN; Nano-sheets; Degradation; Solar-energy

Introduction

The predicted future energy needs are satisfied by solar energy, a promising alternative energy source. Consequently, the conversion of solar energy into a usable form has recently attracted a lot of attention [1-2]. Using semiconducting visible-light-driven photocatalysts to degrade pollutants is seen as a successful strategy for resolving the current pollution issue. Metal-free graphitic carbon nitride (GCN) has gained the most interest among visible-light-driven photocatalysts because of its ideal band structure for the degradation of contaminants, hydrogen generation reaction (HER), high thermal, and chemical stability, and earth abundance [3]. Unfortunately, pure GCN have disadvantages of relatively rapid photo-generated carrier recombination, a low density of active sites, and a small surface area for use in practical applications [4]. Therefore, in this condition, a number of approaches have been devised to address these issues and enhance the photocatalytic activity of GCN. Doping GCN with heteroatoms [5], such as metal and non-metal atoms, is one method [6]. Two-dimensional GCN nanosheets (NSs) have a higher surface area than bulk GCN and can therefore offer more active and adsorption sites for the photocatalytic process [7-8]. The NSs structure can indeed encourage charge carrier mobility at the interface, increasing the photocatalytic activity [9].

Atomic doping is of great interest because it can alter the electrical and optical properties of GCN at the atomic level, such as tuning the band structures. Narrowing the optical bandgaps, and improving charge transport is important, compare to other modification methods like creating heterojunction photocatalysts and morphological engineering [10-11]. Extensive investigations into GCN nonmetal modification have been attempted. For example to improve the quality attributes of GCN [12-13], M. Seredych et al. constructed a composite made of CS, or visible-light photoactive S-doped carbon, which was synthesized from the common polymer (sodium 4-styrene

sulfonate) [14]. For the synthesis of the nanocomposite, a newly established diffusive force-based approach was applied [15-16]. For example, Zou et al. showed that boron doping significantly increased the photo-degradation activity of GCN by introducing boron atoms into the C sites [17-[18]. Fluorine doping, according to Wang et al.'s observation, largely caused C single bond F bonding in the framework, which resulted in a reduced bandgap and a wider range of light absorption [19]. First-principles theoretical research has shown that the interstitial sites of in-planar GCN include atoms that preferentially replace the edge C and N atoms, altering the optical and electrical characteristics of GCN [20-21]. A significant proportion of earlier studies have concentrated on single-doping, but it has been shown that co-doping GCN with two different metal and non-metal atoms, such as P and S co-doping [22-23] (P, Na) co-doping [24], and (C, O) co-doping [25-26], exhibits higher photocatalytic activity and unusual physiochemical characteristics than single element doping. The doping site has been shown to be essential for GCN photocatalytic performance [27-28]. Doing multi-element doping in the GCN matrix and investigating the mechanism underlying the doping-induced increase in photocatalytic activity are hence challenging. As an illustration, Liu et al. created sulphur-doped GCN by processing the high-grade GCN powder at 450 °C environment of gaseous H_2S [17], [29]. It is important to consider the potential environmental and health risks associated with the synthesis of sulphur-assisted activated carbon GCN composites, and to implement appropriate measures to minimize these risks [30-32].

This study is based on the synthesis of activated carbon GCN by the thermal decomposition method, which is modified with the sulphur (S) element for higher photocatalytic activity. The sulphur is accumulated within the layered structure of activated carbon as well as CGN, which altered the charge transfer route, suppressed photogenerated charge recombination, and reduced the optical band gap for the absorption of visible energy. The optimized amount of sulphur is added

together with activated carbon and GCN. Methyl Blue (MB) is used as an investigator dye to evaluate the efficiency of GCN-0.8 using solar energy irradiation. This study offers an exhaustive analysis of sulphur element assistance with activated carbon GCN, which is crucial for the synthesis of innovative photocatalysts.

2. Experimental section

2.1. Materials

Carbamide ((NH2)2CO) commercial used, sulphur power (99.9 %, grade A), carbon tetrachloride (CCl4, 99 %, grade A), ethylene glycol, distilled water, was used as purchased from Sigma Aldrich Pakistan Co, Ltd. (Lahore, Pakistan). The organic dye methyl blue (MB), edta disodium (EDTA-2Na) and isopropyl alcohol (IPA, 99 %, grade A) was likewise obtained from Sigma Aldrich Pakistan Co, Ltd. (Lahore, Pakistan), and used without further purification and modification.

2.2. Synthesis activated carbon GCN

Thin graphitic carbon nitride (GCN) nanosheets with activated carbon were synthesized using thermal decomposition and the secondary-calcination method. Normally, 25 g of carbamide were directly heated in a muffle furnace using a ceramic combustion boat. The annealed temperature was kept at 550 °C for 3 h with a heating rate of 5 °C min^{-1}. Resumed the annealing procedure as described above, allowing the material to cool naturally to room temperature. A yellow-colored power was attained, which further grounded to a fine power obtained for characterizations. The pristine synthesized GCN nano-sheets were identified as activated carbon GCN.

2.3. Synthesis of sulphur assisted activated carbon GCN

The synthesized activated carbon GCN nanosheets and sulphur power in different weight percent ratios, such as (1:0.1, 1:0.2, 1:0.4, 1:0.6, and 1:0.8), were dispersed in a 20 mL carbon tetrachloride. The prepared solution was stirred for 3 h at room temperature. The resulting materials were centrifuged and collected in the form of precipitates. Moreover, it was washed thoroughly several times with distilled water and ethanol. Finally, the product was dried at 80 °C for 24 h before further investigation. The trails classified are called GCN, GCN-0.1, GCN-0.2, GCN-0.4, GCN-0.6, and GCN-0.8, where the numbers represent the sulphur ratio added to the activated carbon GCN.

2.4. Characterization

X-ray Diffraction (XRD) (Philips X'Pert Pro MPD, with X-ray source, 3 kW, Cu Kα (1.5405 Å)) is used to analyze the crystal structures of all the synthesized samples. Scanning electron microscopy (Hitachi S-4800, 1.0 nm resolution at 15 kV, WD = 4 mm, Accelerating Voltage range 0.5 to 30 kV in 100 V steps) was used to examine the elemental weight percentage and microstructure of the synthesized samples. Methyl-Orange (MO) dye degradation was used to evaluate the products' stability and effectiveness ($\lambda > 420$ nm, CEL-HXF300, China Education Au-light, Beijing). In order to examine band gaps and K values, UV–Vis. spectra were recorded using a Shimadzu UV-1700 spectrophotometer. Bandgaps and K values were calculated from these measurements.

3. Result and discussion

3.1. Structural and compositional analysis

The XRD diffraction pattern analysis for crystal structure and phase identification of the activated carbon GCN with sulphur assistance composites is shown in Fig. 1. The broader diffraction peak appeared at 20.0o, which is the consequence of randomly positioned activated carbon aromatic sheets, which confirmed that activated carbon is present in the GCN [33-34]. The distinctive graphitic layered structures that maintain the inter-layer stacking of conjugated system is indicated by the peak positioned at 27.9o, which matches the interlayer at d = 0.327 nm. No extra peak is displayed in the XRD spectra, which attributes that only graphitic nitride and activated carbon is accumulated with sulphur element. It is suggested that, although the crystal structure of the doped material does not change, the phase and lattice constant generally do change, resulting in a slight shift in the diffraction peaks. [35]. Because the intensity of the activated carbon peak decreases as the sulphur amount increases, this could be due to an extra amorphous state appearing due to lattice strain. Furthermore, the nuclide size of the carbon element is significantly smaller compared with the sulphur element, which is a major reason for the induction of lattice strain, amorphous states, and increased crystallite size of the material. Moreover, dropping the peak intensity may be due to the thinning quality of GCN. As a result, as the sulphur quantity increases, the peak intensity at an angle of 27.9o increases, indicating that the crystallinity of the activated carbon GCN increased because the sulphur element has a more crystalline nature, as shown in Fig. 1(b).

The Scanning Electron Microscopy (SEM) analysis is used to characterize microstructures, which enable us to determine the morphology, size, and shape of synthesized particles. It facilitates our comprehension of the physical properties of our material. The SEM analyses of activated

carbon GCN and sulphur assisted composites were carried out. The SEM images for all the samples were recorded as shown in Fig. 2. SEM image of pure activated carbon GCN is shown in Fig. 2(a), which shows the material has thin sheet-like structures. The sulphur assistance with activated carbon GCN is shown in Fig. 2(b-f). As the pure activated carbon GCN-0 displays a two-dimensional structure with a typical irregular porosity and the morphology of flat sheets stacked together with wrinkles and irregular shapes. The nanosheets sticking to each other in the photographs could be the cause of the uneven size distribution of the sheets. The nanosheets become smaller, thicker, and more folded as the sulphur-loaded ratio increases. Furthermore, the specific surface area of the nanosheets may increase as they gradually turn and fold into a round shape. Moreover, energy dispersive x-ray spectroscopy (EDS) offers further insight into the surface material. EDX analysis, which provides chemical composition and elemental study as shown in Fig. 2(g-i), determines a sample's elemental composition.

The EDS spectral analysis results of the selected samples exhibited the existence of elements such as N, C, O and S in the composite material. The oxygen present in the spectrums typically observed and is from the ambient of the instrument. Similarly, the additional spectral peaks with high intensity present in Fig. 2(g-i) may be coming from the sample holder where the sample was placed. In the synthesized material the elemental percentage for GCN-0 is 32.69 %, 59.38, and 06.84 % of C, N, and O, respectively, as displayed in the EDS results. It is interesting to note that the presence of sulphur in the GCN structure has been confirmed, and its amount has been enhanced by adding additional quantities of sulphur to the GCN structure (Fig. 2h and i). Consequently, sulphur element is accumulated with GCN, resulting in higher catalytic sites and enhanced photocatalytic activity.

4. UV–vis analysis

The optical band gap for activated carbon GCN and sulphur assisted composites is measured using UV–Vis diffuse reflectance spectra. Using optical measurements, the light absorption characteristics of semiconductor materials were assessed as shown in Fig. 3. Surprisingly, two band gaps occur: one is for activated carbon element, and the other is due to graphitic carbon nitride, which is mentioned in the XRD spectra. In pure activated carbon GCN, the bandgap energy is 3.31 eV and 3.38 eV, for GCN and activated carbon, respectively. The higher band gap of CGN-0 indicated that carbon contents were added, which increased band gap energy that was outside the range of visible light spectra, resulting no light energy being absorbed for photocatalytic activity. As we loaded sulphur element with the activated carbon GCN, the reduction in band gap arises. The band gap energy for activated carbon GCN is lowered from 3.38 eV to 3.06 eV, whereas for GCN its reduction is from 3.15 eV to 2.84 eV in the samples GCN-0.1, GCN-0.2, GCN-0.4, GCN-0.6, and GCN 0.8, as shown in Fig. 3(b-f). Therefore, it demonstrates how crucial a role the S element play in improving light absorption for enhanced photocatalytic activity. The following mathematical expression is employed for approximating the potential energy of the semiconductor materials.

$$(\alpha h \upsilon)^n = A(h \upsilon - E_g) \quad (1)$$

The bandgap energy, absorption coefficient, frequency, Planck's constant, and band tailing constant are denoted by the following symbols, in that order: Eg, α, υ, h, and A. The power factor of the transition mode, n (2, and 1/2), serves as an indication of the material's characteristics. Its value is 2 for materials with a direct bandgap transition, while 1/2 is represented by an indirect bandgap transition. From the results mentioned in Fig. 3, enhanced solar energy absorption,

attributed to narrow band gap energy. As a consequence, enhanced photocatalytic activity was observed.

5. Photocatalytic activity

To study the photocatalytic activities of the synthesized materials, the common organic dye Methyl Blue (MB), which is commonly employed in the industry, was selected. The trails for photocatalytic degradation were performed at (500 W Xe-lamp, 380 nm, visible light irradiation at ambient temperature). The degradation of prototype dye MB is clearly illustrated in Fig. 4, which shows 26 %, 43 %, 56 %, 73 %, 88 %, and 99 % degradation for the samples GCN-0, GCN-0.1, GCN-0.2, GCN-0.4, GCN-0.6, and GCN-0.8, respectively. The percentage of degradation on sample GCN-0.8 attained the highest level compared to the other trails, even if we increase activated carbon GCN: sulphur ratio to 1:1. The GCN-0.8 is the optimized sample, which has higher photo-catalytic activity, consequence of the accumulation of sulphur contents on the activated carbon. In the development of a satisfactory catalyst, sulphur paid a significant influence. Sulphur, which belongs to the sixth group of periodic table and has more electrons in the valance band, which pushes energy levels close to the conduction band. It facilitates the catalytic behavior's transition from the valence band to the conduction band and alters the charge transfer route, suppressing the photo-generated electron-hole pairs recombination. The activated carbon present in the GCN, as evidenced by the XRD spectra, which elevated the bandgap of the GCN [36]. The low photocatalytic activity of the other samples is due to the activated carbon exiting in the GCN-0. Furthermore, the decreased photocatalytic activity of GCN-0 is linked to increased photo-generated electron-hole recombination and less solar energy absorption [35]. Surprisingly, the MB nearly entirely deteriorated with GCN-0.8 within 80 min. The Langmuir-Hinshelwood model is typically used to determine the photocatalytic degradation kinetics of organic pollutions. Hence, it

is assumed that the catalytic interaction takes place here between absorbed pollutant molecules and photo-generated reactive oxygen vacancies. By allowing that the amount of pollutant molecules absorbed does not depend on their concentration in the medium, the Langmuir-Hinshelwood model is employed as a second-order kinetic model, which is further simplified to a pseudo-first-order kinetic [37]. Consequently, the pseudo-first-order reaction constant (k) for GCN-0.8 was evaluated as shown in Fig. 4(c-d). In the logarithmic form, the first order kinetic reaction constant (k) is determined using mathematical expression (2).

$$Ln\left(\frac{Co}{C}\right)^{n} = -Kt \qquad (2)$$

wherein, k is the kinetic reaction constant, C_o (initial) and C (verified) concentration for MB, and t (min) is the time of reaction. The experimentally evaluated values of k for GCN-0, GCN-0.1, GCN-0.2, GCN-0.4, GCN-0.6, and GCN-0.8 are 3.5×10^{-3}, 7.0×10^{-3}, 9.9×10^{-3}, 1.5×10^{-2}, 2.2×10^{-2}, and 4.1×10^{-2}, respectably. The optimum quantity of sulphur assisted with the activated carbon GCN regulated the charge transfer route and enhanced the optical absorption, indicated by a large k value, resulting in higher photocatalytic activity.

6. Photocatalytic mechanism

The afore-mentioned evaluation and experimentation observations provided a detailed explanation of the photocatalytic degradation process. Results demonstrate that the synthesized samples of GCN have varying photo-absorption capabilities while maintaining the same shape and phase composition, as indicated above. Because of this, the accumulation of sulphur element with porous layered structures of GCN has the exceptional ability to facilitate efficient charge separation and transfer from the bulk to the outer surface of the layers. The optimized GCN trial is an essential

step for suppression of photo-generated electron-hole pairs and improved photocatalytic efficiency. Additionally, the degree of GCN nanosheet thickness, crystallinity, and altering the charge transfer route through sulphur element may be crucial factors for photocatalytic activity [38]. Surface imperfections had a big impact on how nanomaterials behaved chemically and physically. Due to the solar energy irradiation upon the photo-catalysts, oxygen vacancies (OVs) can be produced on the surface of GCN [39], which is possible due to the unique layer structure and relatively low materialization energy [40]. The localized states of generated oxygen vacancies may improve visible light responsiveness and serve as activation centers and sites for adsorption, which increases photocatalytic activity [41]. The GCN-0.8 sample, which has been optimized for outstanding MB degradation performance, as shown in Fig. 5(a-b). According to our previous studies, the sulphur GCN composites demonstrated remarkable photodegradation performance for MB. This is due to secondary level states produced at conduction band minima near positive potential and valence band maxima in GCN and activated carbon. Moreover, the bandgap is reduced with sulphur addition, which is attributed to higher optical energy absorption. The band gap for activated is reduced from 3.38 eV to 3.06 eV, and since the optical absorption is started at 3.1 eV, this confirms that three samples, such as GCN-0.4, GCN-0.6, and GCN-0.8, have the ability to absorb visible light energy. On the other hand, the band gap of graphitic carbon nitride is reduced from 3.31 eV to 2.84 eV, indicating that all trials absorbed visible energy except the GCN sample. The combined effect of activated carbon and graphitic carbon nitride encouraged a large range of optical energy to be absorbed from a higher energy region to a lower one, resulting in higher photocatalytic activity being achieved.

Since the activated carbon is made up of a complex matrix, with a larger sulphur concentration would seem to result in enhanced photocatalytic activity [42], [43]. Sulphur-

functional organic groups, such as sulphur in aromatic rings, are thought to be responsible for the photoactivity of sulphur-assisted activated carbon [44]. Sulphur likely causes the band gap to narrow and electron-hole pairs to develop. Researchers have looked at the physics of band-gap reduction in a variety of materials, including nanocrystals and nanocomposites [45]. Furthermore, GCN and sulphur exhibit excellent pollutant degradation efficiency [46]. Moreover, activated carbon GCN and sulphur assistance have a synergistic effect on methyl blue degradation. We also conducted a stability test, as depicted in Fig. 5b, which revealed a slight reduction over the course of four successive cycles, demonstrating the outstanding stability of photocatalysts.[47].

7. Conclusion

In this article, we examine the thermal decomposition of commercially used urea to synthesized activated carbon CGN with sulphur composites. The specific ratio of sulphur with GCN is employed for the degradation of methyl blue. The accumulation of sulphur with the activated carbon and GCN decreased the bandgap of the materials and a photogenerated electron-hole pair transfer channel, which decreased photogenerated charge recombination and enhanced the photocatalytic performance. The degradation of synthetic organic methyl blue dye was investigated for all the synthesized samples, it was discovered that GCN-0.8 demonstrated improved catalytic efficiency as a result of its reduced band gap, higher crystallinity and reduced charge transfer impedance. The optical energy bandgap of activated carbon GCN-0.8 was estimated to be 2.84 eV, and the GCN-0.8 first-order kinetic constant led to improved solar energy absorption and increased MB photocatalytic degradation efficiency. This study also identifies useful photocatalysts that may clean up organic contaminants when exposed to visible light energy.

Acknowledgements

The authors are grateful for the financial support by the National Natural Science Foundation of China (51602281), Natural Science Foundation of Shandong Province (No: ZR2019MEM025), Innovative Science and Technology Platform Project of Cooperation between Yangzhou City and Yangzhou University, China (No. YZ202026308), Yangzhou University self-made experimental equipment special fund (YZUZZ2022-13), Yangzhou University High-end Talent Support Program and the "Qinglan Project" of Jiangsu University. The authors would also like to thank the Researchers Supporting Project Number (RSPD-2023R668), King Saud University, Riyadh, Saudi Arabia.

References

[1] H.J. Kong, D.H. Won, J. Kim, S.I. Woo, Sulfur-doped g-C3N4/BiVO4 composite photocatalyst for water oxidation under visible light, Chem. Mater. 28 (2016)1318–1324.

[2] A. Hussain, J. Hou, M. Tahir, S. Ali, Z.U. Rehman, M. Bilal, T. Zhang, Q. Dou, X. Wang, Recent advances in BiOX-based photocatalysts to enhanced efficiency for energy and environment applications, Catal. Rev. (2022) 1–55.

[3] J. Hou, M. Yang, Q. Dou, Q. Chen, X. Wang, C. Hu, R. Paul, Defect engineering in polymeric carbon nitride with accordion structure for efficient photocatalytic CO_2 reduction and H2 production, Chem. Eng. J. 450 (2022), 138425.

[4] C. Ye, J.-X. Li, Z.-J. Li, X.-B. Li, X.-B. Fan, L.-P. Zhang, B. Chen, C.-H. Tung, L.-Z. Wu, Enhanced driving force and charge separation efficiency of protonated g-C3N4 for photocatalytic O2 evolution, ACS Catal. 5 (2015) 6973–6979.

[5] H. Jiang, Y. Li, D. Wang, X. Hong, B. Liang, Recent advances in heteroatom doped graphitic carbon nitride (g-C3N4) and g-C3N4/metal oxide composite photocatalysts, Curr. Org. Chem. 24 (2020) 673–693.

[6] Y. Yu, K. Wu, W. Xu, D. Chen, J. Fang, X. Zhu, J. Sun, Y. Liang, X. Hu, R. Li, Adsorption-photocatalysis synergistic removal of contaminants under antibiotic and Cr (VI) coexistence environment using non-metal g-C3N4 based nanomaterial obtained by supramolecular self-assembly method, J. Hazard. Mater. 404 (2021),

124171.

[7] Q. Dou, J. Hou, A. Hussain, G. Zhang, Y. Zhang, M. Luo, X. Wang, C. Cao, One-pot synthesis of sodium-doped willow-shaped graphitic carbon nitride for improved photocatalytic activity under visible-light irradiation, J. Colloid Interface Sci. 624 (2022) 79–87.

[8] J. Hou, T. Zhang, T. Jiang, X. Wu, Y. Zhang, M. Tahir, A. Hussain, M. Luo, J. Zou, X. Wang, Fast preparation of oxygen vacancy-rich 2D/2D bismuth oxyhalides-reduced graphene oxide composite with improved visible-light photocatalytic properties by solvent-free grinding, J. Clean. Prod. 328 (2021), 129651.

[9] D. Liu, S. Zhang, J. Wang, T. Peng, R. Li, Direct Z-scheme 2D/2D photocatalyst based on ultrathin g-C3N4 and WO3 nanosheets for efficient visible-light-driven H_2 generation, ACS Appl. Mater. Interfaces 11 (2019) 27913–27923.

[10] J. Hou, T. Jiang, X. Wang, G. Zhang, J.-J. Zou, C. Cao, Variable dimensional structure and interface design of g-C3N4/BiOI composites with oxygen vacancy for improving visible-light photocatalytic properties, J. Clean. Prod. 287 (2021),125072.

[11] J. Hou, X. Tu, X. Wu, M. Shen, X. Wang, C. Wang, C. Cao, H. Pang, G. Wang, Remarkable cycling durability of lithium-sulfur batteries with interconnected mesoporous hollow carbon nanospheres as high sulfur content host, Chem. Eng. J. 401 (2020), 126141.

[12] T. Zhang, L. Chen, T. Jiang, J. Hou, G. Zhang, A. Hussain, Chemical precipitation synthesis of Bi0.7Fe0.3OCl nanosheets via Fe (III)-doped BiOCl for highly visible light photocatalytic performance, Mater. Today Commun. 26 (2021), 102145.

[13] K. Devarayapalli, K. Lee, H.-B. Do, N. Dang, K. Yoo, J. Shim, S.P. Vattikuti, Mesostructured g-C3N4 nanosheets interconnected with V2O5 nanobelts as electrode for coin-cell-type-asymmetric supercapacitor device, Mater. Today Energy 21 (2021), 100699.

[14] M. Seredych, S. Łoś, D.A. Giannakoudakis, E. Rodríguez-Castellón, T.J. Bandosz, Photoactivity of g-C3N4/S-doped porous carbon composite: synergistic effect of composite formation, ChemSusChem 9 (2016) 795–799.

[15] J. Xu, L. Zhang, R. Shi, Y. Zhu, Chemical exfoliation of graphitic carbon nitride for efficient heterogeneous photocatalysis, J. Mater. Chem. A 1 (2013) 14766–14772.

[16] Z.U. Rehman, M. Bilal, J. Hou, F.K. Butt, J. Ahmad, S. Ali, A. Hussain, Photocatalytic CO2 reduction using TiO2-based photocatalysts and TiO2 Z-scheme heterojunction composites: a review, Molecules 27 (2022) 2069.

[17] G. Liu, P. Niu, C. Sun, S.C. Smith, Z. Chen, G.Q. Lu, H.-M. Cheng, Unique electronic structure induced high photoreactivity of sulfur-doped graphitic C3N4, J. Am. Chem. Soc. 132 (2010) 11642–11648.

[18] G. Murali, S.P. Vattikuti, Y.K. Kshetri, H. Lee, J.K.R. Modigunta, C.S. Reddy, S. Park, S. Lee, B. Poornaprakash, H. Lee, Near-infrared-activated Z-scheme NaYF4: Yb/Tm@ Ag3PO4/Ag@ g-C3N4 photocatalyst for enhanced H2 evolution under simulated solar light irradiation, Chem. Eng. J. 421 (2021), 129687.

[19] Y. Wang, Y. Di, M. Antonietti, H. Li, X. Chen, X. Wang, Excellent visible-light photocatalysis of fluorinated polymeric carbon nitride solids, Chem. Mater. 22 (2010) 5119–5121.

[20] X. Ma, Y. Lv, J. Xu, Y. Liu, R. Zhang, Y. Zhu, A strategy of enhancing the photoactivity of g-C3N4 via doping of nonmetal elements: a first-principles study, J. Phys. Chem. C 116 (2012) 23485–23493.

[21] J. Hou, T. Jiang, R. Wei, F. Idrees, D. Bahnemann, Ultrathin-layer structure of BiOI microspheres decorated on N-doped biochar with efficient photocatalytic activity, Front. Chem. 7 (2019) 378–387.

[22] C. Hu, W.-Z. Hung, M.-S. Wang, P.-J. Lu, Phosphorus and sulfur codoped g-C3N4 as an efficient metal-free photocatalyst, Carbon 127 (2018) 374–383.

[23] Z. Rehman, F.K. Butt, N. Balayeva, F. Idrees, J. Hou, Z. Tariq, S. Rehman, B. Haq, S. Alfaify, S. Ali, S. Zaman, A. Hussain, Two-dimensional graphitic carbon nitride nanosheets as prospective material for photocatalytic degradation of nitrogen oxides, Diam. Relat. Mater. 120 (2021) 108650–108658.

[24] S. Cao, Q. Huang, B. Zhu, J. Yu, Trace-level phosphorus and sodium co-doping of g- C3N4 for enhanced photocatalytic H2 production, J. Power Sources 351 (2017) 151–159.

[25] J. Wu, N. Li, X.-H. Zhang, H.-B. Fang, Y.-Z. Zheng, X. Tao, Heteroatoms binary-doped hierarchical porous g-C3N4 nanobelts for remarkably enhanced visible-light-driven hydrogen evolution, Appl. Catal. B Environ. 226 (2018) 61–70.

[26] S.P. Vattikuti, P.A.K. Reddy, J. Shim, C. Byon, Visible-light-driven photocatalytic activity of SnO2–ZnO quantum dots anchored on g-C3N4 nanosheets for photocatalytic pollutant degradation and H2 production, ACS Omega 3 (2018) 7587–7602.

[27] B. Zhu, J. Zhang, C. Jiang, B. Cheng, J. Yu, First principle investigation of halogen-doped monolayer g-C3N4 photocatalyst, Appl. Catal. B Environ. 207 (2017) 27–34.

[28] B.-X. Zhou, S.-S. Ding, B.-J. Zhang, L. Xu, R.-S. Chen, L. Luo, W.-Q. Huang, Z. Xie, A. Pan, G.-F. Huang, Dimensional transformation and morphological control of graphitic carbon nitride from water-based supramolecular assembly for photocatalytic hydrogen evolution: from 3D to 2D and 1D nanostructures, Appl. Catal. B Environ. 254 (2019) 321–328.

[29] Y.-Y. Li, Y. Si, E.-X. Han, W.-Q. Huang, W. Hu, A. Pan, X. Fan, G.-F. Huang, Steering charge kinetics boost the photocatalytic activity of graphitic carbon nitride: heteroatom-mediated spatial charge separation and transfer, J. Phys. D. Appl.Phys. 53 (2019) 15502.

[30] Y.-Y. Li, B.-X. Zhou, H.-W. Zhang, T. Huang, Y.-M. Wang, W.-Q. Huang, W. Hu, A. Pan, X. Fan, G.-F. Huang, A host–guest self-assembly strategy to enhance π-electron densities in ultrathin porous carbon nitride nanocages toward highly efficient hydrogen evolution, Chem. Eng. J. 430 (2022), 132880.

[31] Y.-Y. Li, Y. Si, B.-X. Zhou, T. Huang, W.-Q. Huang, W. Hu, A. Pan, X. Fan, G.-F. Huang, Interfacial charge modulation: carbon quantum dot implanted carbon nitride double-deck

nanoframes for visible-light photocatalytic tetracycline degradation, Nanoscale 12 (2020) 3135-3145.

[32] B.X. Zhou, S.S. Ding, K.X. Yang, J. Zhang, G.F. Huang, A. Pan, W. Hu, K. Li, W.Q. Huang, Generalized synthetic strategy for amorphous transition metal oxides-based 2D heterojunctions with superb photocatalytic hydrogen and oxygen evolution, Adv. Fun. Mater. 31 (2021), 2009230.

[33] Q. Xu, B. Cheng, J. Yu, G. Liu, Making co-condensed amorphous carbon/g-C3N4 composites with improved visible-light photocatalytic H2-production performanceusing Pt as cocatalyst, Carbon 118 (2017) 241–249.

[34] C. Chen, T. Jiang, J. Hou, T. Zhang, G. Zhang, Y. Zhang, X. Wang, Oxygen vacancies induced narrow band gap of BiOCl for efficient visible-light catalytic performance from double radicals, J. Mater. Sci. Technol. 114 (2022) 240–248.

[35] X. Bai, L. Wang, Y. Wang, W. Yao, Y. Zhu, Enhanced oxidation ability of g-C3N4 photocatalyst via C60 modification, Appl. Catal. B Environ. 152 (2014) 262–270.

[36] M. Mohan, V.K. Sharma, E.A. Kumar, V. Gayathri, Hydrogen storage in carbon materials—a review, Energy Storage 1 (2019), e35.

[37] A. Hussain, J. Hou, M. Tahir, X. Wang, M.U. Qadri, X. Tu, T. Zhang, Q. Dou, J. Zou, Fine-tuning internal electric field of BiOBr for suppressed charge recombination, J. Environ. Chem. Eng. 9 (2021), 104766.

[38] A. Hussain, N. Ali, S. Ali, J. Hou, I. Aslam, H. Naeem, M. Boota, M. Ul-Hussan, J. Yin, X. Wang, Diverse morphological study for nonmetal-doped g-C3N4 composites with narrow bandgap for improved photocatalytic activity, Res. Chem. Intermediat. 48 (2022) 2857–2870.

[39] F. Hasanvandian, M. Moradi, S.A. Samani, B. Kakavandi, S.R. Setayesh,M. Noorisepehr, Effective promotion of g-C3N4 photocatalytic performance via surface oxygen vacancy and coupling with bismuth-based semiconductors toward santibiotics degradation, Chemosphere 287 (2022), 132273.

[40] S.P. Vattikuti, C. Byon, Hydrothermally synthesized ternary heterostructured MoS2/Al2O3/ g-C3N4 photocatalyst, Mater. Res. Bull. 96 (2017) 233–245.

[41] S. Zhang, Y. Liu, R. Ma, D. Jia, T. Wen, Y. Ai, G. Zhao, F. Fang, B. Hu, X. Wang, Molybdenum (VI)-oxo clusters incorporation activates g-C3N4 with simultaneously regulating charge transfer and reaction centers for boosting photocatalytic performance, Adv. Funct. Mater. 32 (2022), 2204175.

[42] J. Song, Z. Meng, X. Wang, G. Zhang, C. Bi, J. Hou, One-step microwave method synthesis of Fe3O4 nanoribbon@ carbon composite for Cr (VI) removal, Sep. Purif. Technol. 298 (2022), 121530.

[43] J. Hou, R. Wei, X. Wu, M. Tahir, X. Wang, F. Butt, C. Cao, Lantern-like bismuth oxyhalides embedded typha-based carbon via in-situ self-template and ion exchange-recrystallization for high-performance photocatalysis, Dalton Trans. 47 (2018) 6692–6701.

[44] J. Matos, J. Laine, J.-M. Herrmann, D. Uzcategui, J. Brito, Influence of activated carbon upon titania on aqueous photocatalytic consecutive runs of phenol photodegradation, Appl. Catal. B Environ. 70 (2007) 461–469.

[45] X. Chen, L. Liu, P.Y. Yu, S.S. Mao, Increasing solar absorption for photocatalysis with black hydrogenated titanium dioxide nanocrystals, Science 331 (2011)746–750.

[46] A. Hussain, S. Maqsood, R. Ji, Q. Zhang, M. Umer Farooq, M. Boota, M. Umer, M. Hashim, H. Naeem, Z. Toor, A. Ali, J. Hou, Y. Xue, X. Wang, Investigation of transition metal-doped graphitic carbon nitride for MO dye degradation, Diam. Relat. Mater. 132 (2023) 109648–109655.

Graphical Abstract

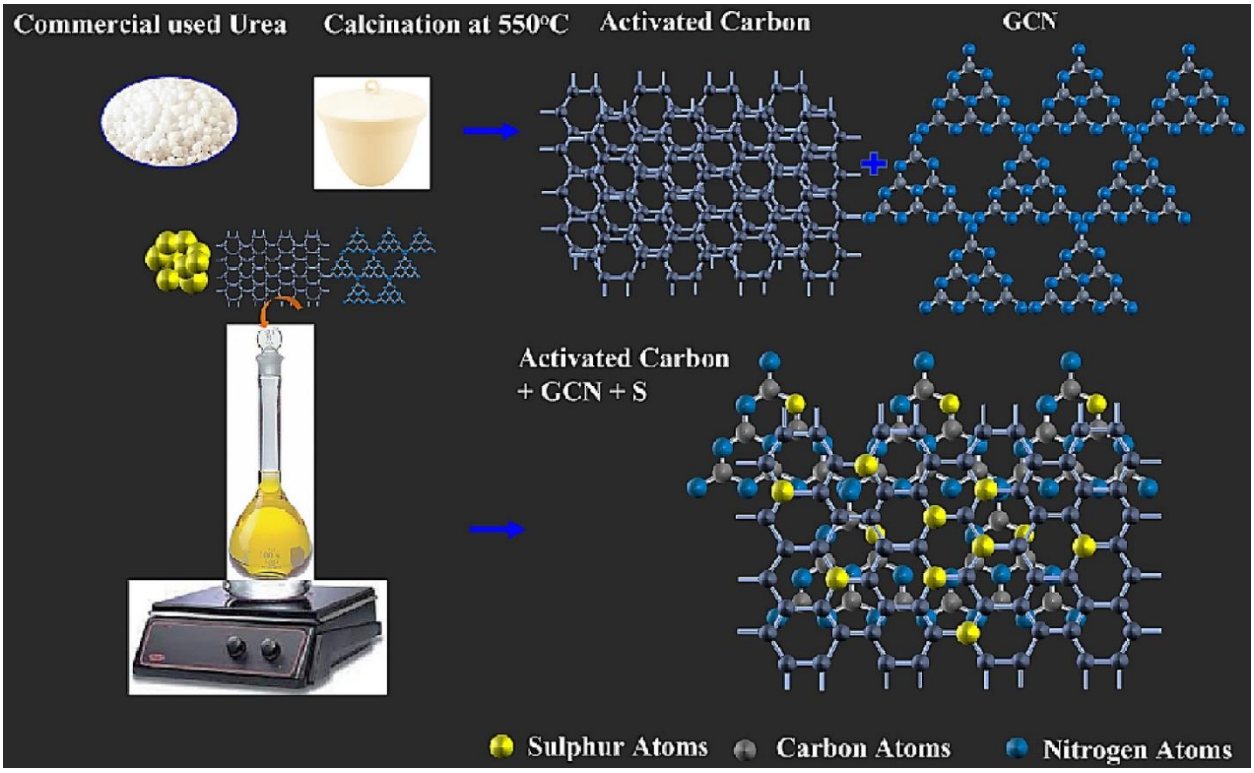

Diagram. Schematic diagram activated carbon GCN with sulphur (illustrating section 2.3).

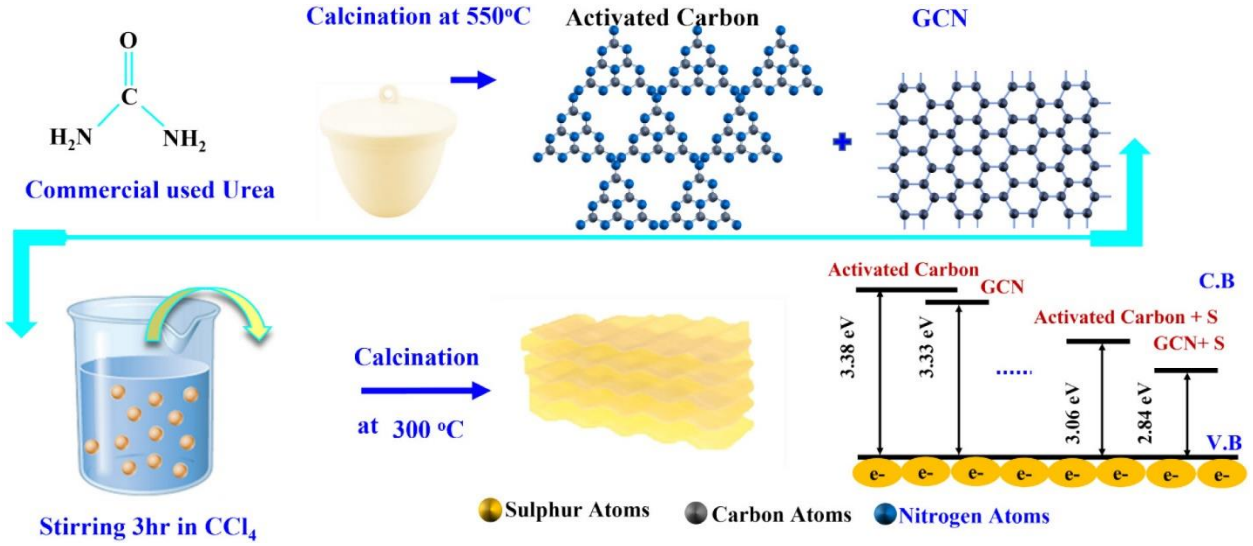

Fig. 1. XRD characteristics spectra for (a) activated carbon GCN with sulphur assistance and (b) local enlarged view.

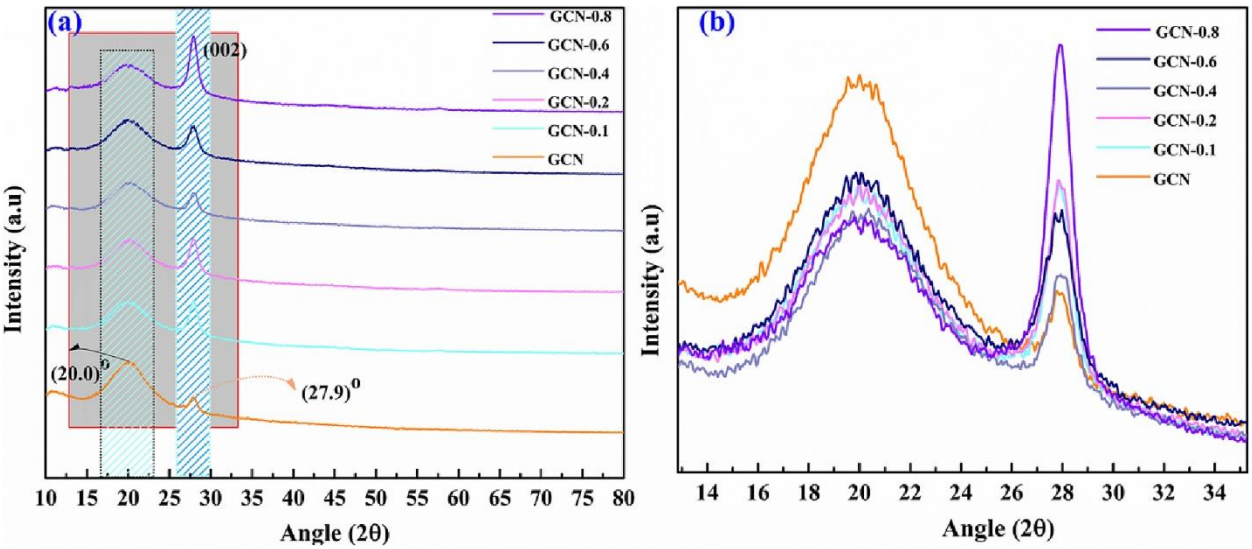

Fig. 2. Scanning electron microscopy (a-f) and EDS for GCN-0, GCN-0.4, and GCN-0.8 (g-i).

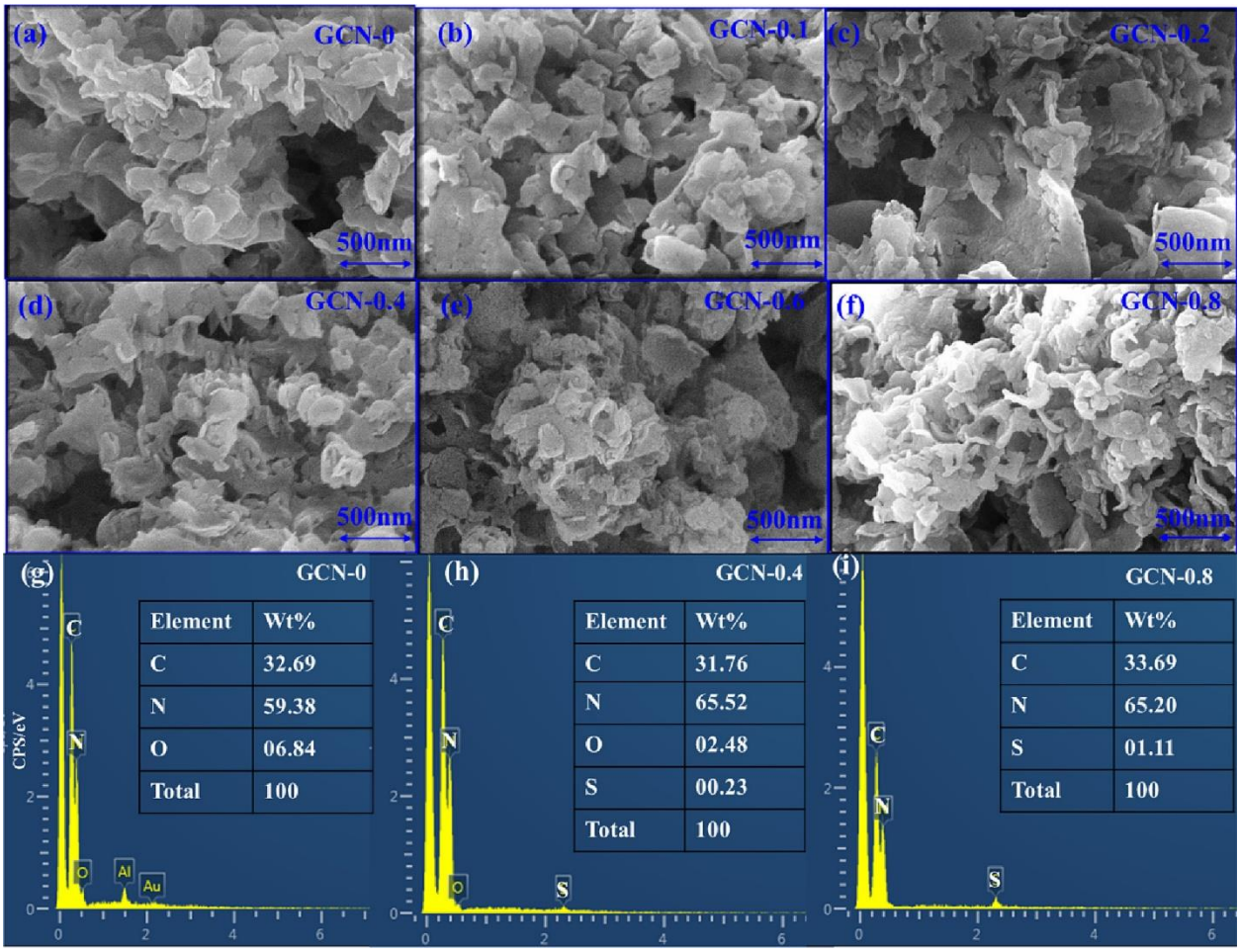

Figure 3 Optical bandgap energy for activated carbon GCN and sulphur assisted GCN composites (a-f).

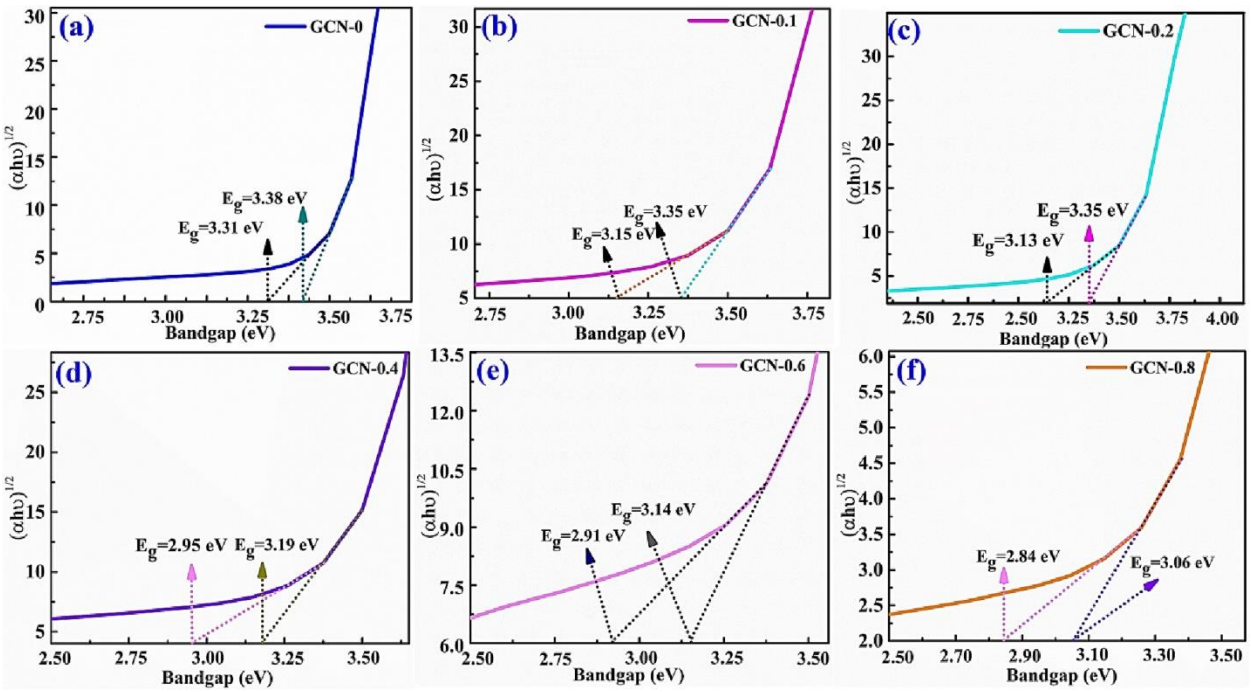

Fig. 4. Methyl Blue Photo-degradation (a), Degradation percentage (%) (b), First-Order Kinetic Constant (K) (c), $Ln\left(\frac{Co}{C}\right)^{n}$ Vs 't' graph (d).

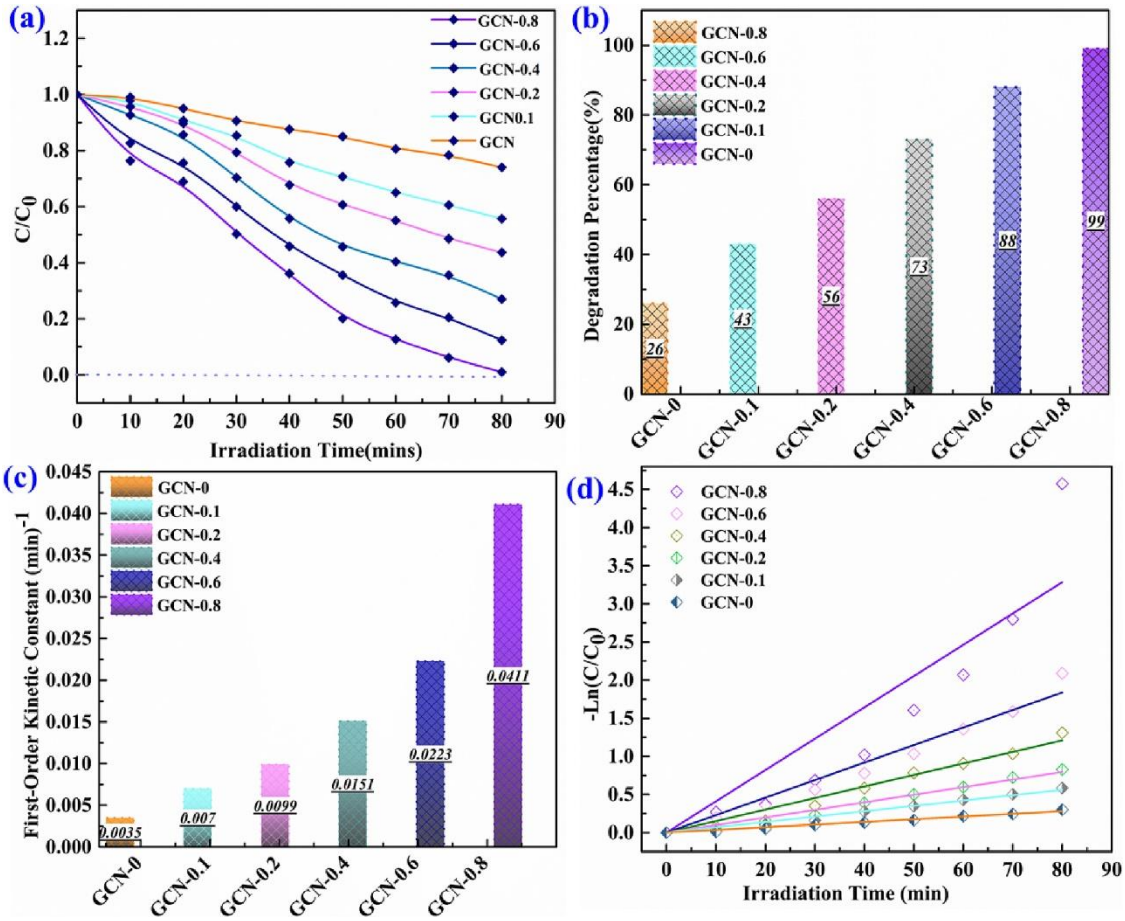

Fig. 5. Activated carbon GCN band gap variation with sulphur loading (a), stability test for GCN-0.8 (b).